

Laser-Induced Particle Adsorption on Atomically Thin MoS₂

Bien Cuong Tran Khac,[†] Ki-Joon Jeon,[‡] Seung Tae Choi,^{†,⊥} Yong Soo Kim,[§] Frank W. DelRio,^{||} and Koo-Hyun Chung^{*,†}

[†]School of Mechanical Engineering, University of Ulsan, Ulsan 44610, Republic of Korea

[‡]Department of Environmental Engineering, Inha University, Incheon 22212, Republic of Korea

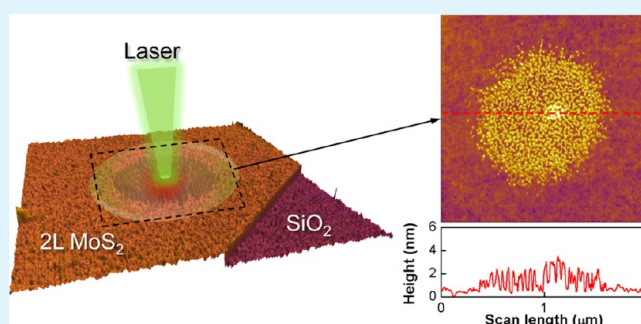
[§]Department of Physics and Energy Harvest Storage Research Center, University of Ulsan, Ulsan 44610, Republic of Korea

^{||}Applied Chemicals and Materials Division, Material Measurement Laboratory, National Institute of Standards and Technology, Boulder, Colorado 80305, United States

Supporting Information

ABSTRACT: Atomically thin molybdenum disulfide (MoS₂) shows great potential for use in nanodevices because of its remarkable electronic, optoelectronic, and mechanical properties. These material properties are often dependent on the thickness or the number of layers, and hence Raman spectroscopy is widely used to characterize the thickness of atomically thin MoS₂ due to the sensitivity of the vibrational spectrum to thickness. However, the lasers used in Raman spectroscopy can increase the local surface temperature and eventually damage the upper layers of the MoS₂, thereby changing the aforementioned material properties. In this work, the effects of lasers on the topography and material properties of atomically thin MoS₂ were systematically investigated using Raman spectroscopy and atomic force microscopy. In detail, friction force microscopy was used to study the friction characteristics of atomically thin MoS₂ as a function of laser powers from 0.5 to 20 mW and number of layers from 1 to 3. It was found that particles formed on the top surface of the atomically thin MoS₂ due to laser-induced thermal effects. The degree of particle formation increased as the laser power increased, prior to the thinning of the atomically thin MoS₂. In addition, the degree of particle formation increased as the number of MoS₂ layers increased, which suggests that the thermal behavior of the supported MoS₂ may differ depending on the number of layers. The particles likely originated from the atmosphere due to laser-induced heating, but could be eliminated via appropriate laser powers and exposure times, which were determined experimentally. The outcomes of this work indicate that thermal management is crucial in the design of reliable nanoscale devices based on atomically thin MoS₂.

KEYWORDS: adsorbates, friction force microscopy, laser power, Raman spectroscopy, thermal conductivity



INTRODUCTION

Atomically thin molybdenum disulfide (MoS₂) has attracted tremendous interest because of remarkable material properties that differ from those of the bulk form. For example, the indirect bandgap in bulk MoS₂ gradually increases up to the direct band gap in a form of monolayer,¹ which suggests the great potential of monolayer MoS₂ for use in nanoscale electronic^{2,3} and optoelectronic^{4,5} devices. Various chemical sensors have also been proposed based on changes to the electronic properties of atomically thin MoS₂ because of adsorbates.^{6,7} In addition, the superior mechanical properties of atomically thin MoS₂ further suggest its potential applicability for use in nanoscale devices.^{8,9} Furthermore, low frictional characteristics of MoS₂^{10–12} allow for the exploitation of atomically thin MoS₂ as a protective or lubricant layer,^{13,14} especially for devices that encounter a contact sliding during operation.

The material properties of atomically thin MoS₂ are often dependent on thickness or the number of layers. Raman spectroscopy has been widely utilized to characterize the thickness of atomically thin MoS₂ and the material properties associated with thickness because of the sensitivity of the vibrational spectrum to thickness.^{15,16} Also, thermal conductivity of atomically thin MoS₂ has been obtained based on the relationship between frequency shift of Raman characteristic peaks and temperature.^{17–22} Thermal effects caused by the laser during Raman spectral measurements have also been reported. For example, thickness-dependent shifts in the Raman modes of atomically thin MoS₂ because of laser-induced thermal effects have been observed.²³ In particular, the upper layers of the MoS₂ can be removed under high laser power and

Received: October 4, 2015

Accepted: January 21, 2016

Published: January 21, 2016

the fabrication of monolayer MoS₂ was demonstrated based on laser ablation.^{24,25} Furthermore, it was shown that the treatment using a pulsed laser may cause damage on the MoS₂ surface.²⁶ In fact, high-powered lasers often cause increases in the local temperature at the surface,^{27–29} and therefore surface damage may occur. To minimize thermal effects on atomically thin MoS₂ during Raman spectral measurements, a wide range of laser powers from 0.14 to 2 mW are used.^{16,18,19,21,24} However, the effects of lasers on the surface of atomically thin MoS₂ have not been explored.

In this work, the effects of lasers on the surface of atomically thin MoS₂ are systematically investigated using Raman spectroscopy and atomic force microscopy (AFM). Atomically thin MoS₂ with various thicknesses were treated with a laser at powers ranging from 0.5 to 20 mW using Raman spectroscopy, and the surfaces of treated regions were then carefully observed by AFM. In particular, friction force microscopy (FFM) images clearly demonstrate the effects of laser treatment on the surface of atomically thin MoS₂. It is demonstrated that particles may be formed on the top surface of atomically thin MoS₂ because of laser-induced thermal effects as functions of layer thickness and laser power. Such particle formation, which may degrade the electronic and optoelectronic properties of atomically thin MoS₂, should be taken into account for the design of reliable nanodevices using atomically thin MoS₂. This observation is also of importance for a comprehensive understanding of the thermal effect on the surface of atomically thin MoS₂. In addition, from FFM, the friction characteristics were quantitatively assessed to gain a better understanding of the friction properties of atomically thin MoS₂, considering that the friction characteristics of atomically thin MoS₂ have not been intensively explored, in contrast to graphene.^{30–33} A quantitative understanding of the friction characteristics of atomically thin MoS₂ provides useful information to elucidate the feasibility of atomically thin MoS₂ as protective or lubricant layers for nanoscale devices.

■ EXPERIMENTAL SECTION

MoS₂ flakes from natural crystalline MoS₂ (SPI supplies) were deposited onto an SiO₂/Si substrate by mechanical exfoliation.^{6,34} The thickness of the thermally grown SiO₂ substrate layer was about 280 nm. The number of MoS₂ layers on the substrate was identified by optical microscopy (VK-X200, Keyence), AFM (MFP-3D, Asylum Research), and Raman spectroscopy (Alpha300R, Witec). All specimens were carefully examined using optical microscopy and AFM observations, prior to the experiment, to ensure that the specimens were free from tape residue. Also, the chemical state of the MoS₂ specimen was analyzed by X-ray photoelectron spectroscopy (XPS, PHI Quantera II, Physical Electronics) to assess the degree of contamination from the mechanical exfoliation process. The topographies of specimens were obtained from the intermittent contact mode of AFM using silicon probes with a nominal normal spring constant of 2 N/m (AC240, Olympus). After intermittent contact mode imaging, contact mode imaging was performed to observe thermal effects on friction properties of the atomically thin MoS₂ and to observe the movement of particles caused by the probe. Silicon probes with a nominal spring constant of 0.2 N/m (LFMR, Nanosensors) were used for contact mode imaging. For quantitative force measurement, normal³⁵ and lateral³⁶ force calibrations were performed prior to contact mode imaging. The normal force for contact mode imaging was initially set to 0.5 nN to minimize damage to the AFM probe and specimens during measurements. However, to observe particle movement with respect to the applied normal force, the normal force was increased up to 15 nN.

After careful location and focusing of the laser spot on each specimen, the Raman emission was collected with a 50X objective (NA = 0.8). A laser with an excitation wavelength of 532 nm was used and the spectral resolution of the instrument was set to be 1.4 cm⁻¹. To identify the number of layers, Raman spectra were obtained with a laser power of 0.5 mW and an exposure time of 10 s. However, for laser treatments, the laser power was increased up to 20 mW and the exposure time varied from 10 to 60 s. Laser power was directly measured using a laser power meter and carefully adjusted prior to each laser treatment. The intervals between treatments were about 10 min. All experiments were performed in ambient conditions (25 °C and 40% RH for laser treatments and Raman spectral measurements, and 25–27 °C and 35–45% RH for AFM measurements).

■ RESULTS AND DISCUSSION

Figure 1a shows optical microscopy images of monolayer (1L), bilayer (2L), trilayer (3L), and bulk MoS₂ specimens before laser treatment. These images clearly show differences in optical contrast with respect to the number of layers. Topographic images of specimens obtained under the intermittent contact mode of AFM are shown in Figure 1b, along with cross-sectional height profiles. The thickness of the 1L MoS₂ was about 0.9 nm, which is greater than the theoretical value of thickness for 1L MoS₂ (0.62 nm). This discrepancy may be due to the presence of adsorbents below the MoS₂ layer or interactions between the MoS₂ layers and the substrate,^{15,16} in addition to measurement uncertainty in AFM topography.³⁷ The thicknesses of the 2L and 3L MoS₂ were, respectively, 1.6 and 2.2 nm, which shows step heights of individual layers of 0.6–0.7 nm. This value is comparable with the theoretical interlayer spacing of 1L MoS₂. The thickness of the bulk MoS₂ was about 100 nm, which indicates that the number of layers in the bulk MoS₂ is more than 100. XPS spectra obtained from the as-exfoliated bulk MoS₂ show an extremely small peak associated with carbon (in low concentration), which is likely to originate from the environment,³⁸ in addition to the peaks associated with MoS₂ and SiO₂ (Figure S1). The presence of carbon after mechanical exfoliation is typically observed in previous studies.^{38,39} This indicates that the degree of contamination on the specimen used in this work is comparable to that of other MoS₂ specimens prepared by mechanical exfoliation.

FFM images of MoS₂ specimens obtained under the contact mode of AFM with 5 nN normal force are shown in Figure 1c. Only FFM images obtained from forward scanning (left to right), where darker (brighter) contrast indicates lower (higher) friction force, are shown in the figure. Figure 1c clearly shows that the MoS₂ layer has significantly lower friction force compared to the substrate. The friction forces on the 1L, 2L, and 3L MoS₂ were 0.99 nN, 0.86 nN, and 0.73 nN under 5 nN normal force, respectively. In general, the friction force on atomically thin MoS₂ decreased as the number of layers increased, which agrees with results reported in a previous study.¹¹ The friction force on the bulk MoS₂ was about 0.44 nN, which is significantly smaller than that on the atomically thin MoS₂.

Raman spectroscopy was also used to identify the number of MoS₂ layers. To minimize the thermal effect,^{17,23} the Raman spectra of MoS₂ specimens were obtained with 0.5 mW laser power for 10 s. Figure 1d shows the Raman spectra of the MoS₂ specimens, which represents the dependence of the two Raman modes, E_{2g}¹ and A_{1g}¹, on thickness. As the thickness increased, the frequency of the E_{2g}¹ mode decreased (red-shift) while that of the A_{1g}¹ mode increased (blue-shift), eventually converging

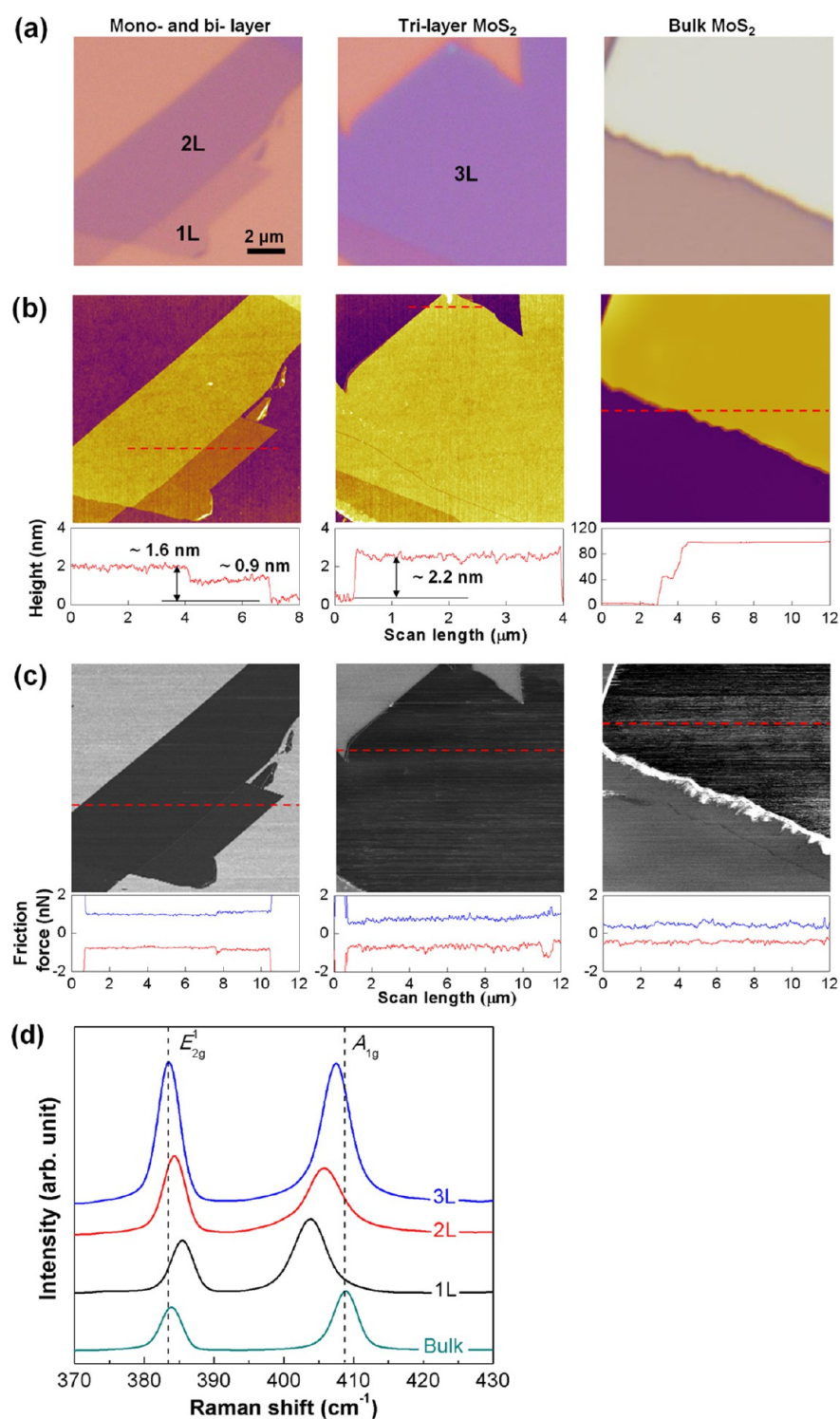


Figure 1. (a) Optical microscopy images, (b) AFM topographic images, (c) FFM images, and (d) Raman spectra of 1L, 2L, 3L, and bulk MoS₂ specimens. The topographic and FFM images were obtained from the intermittent contact and contact modes of AFM, respectively. The cross-sectional profile and the friction loop are included in panels b and c, respectively. The red dashed lines indicate the locations where the cross-sectional profiles and friction loops are taken. For 1L, 2L, and 3L MoS₂, the cross-sectional profiles were obtained from high magnification topographic images for accurate determination of their thickness. FFM images from only the forward scan are included for clarity, where darker (brighter) contrast indicates lower (higher) friction force. The friction loops were obtained from both the forward and backward scanning. In panel d, the frequency of the characteristic peaks of the E_{2g}^1 and A_{1g} modes from the bulk MoS₂ are denoted as dashed lines for comparison.

on the frequency values of the bulk, which is again consistent with a previous study.¹⁶

After characterizations of the thickness and initial states of the surfaces of the MoS₂ specimens using AFM and Raman

spectroscopy, specimens were exposed to the laser at different powers to investigate the surface damage of atomically thin MoS₂. Initially, laser power varied by 1 mW, 5 mW, and 10 mW while the exposure time was set to 60 s. After laser treatment,

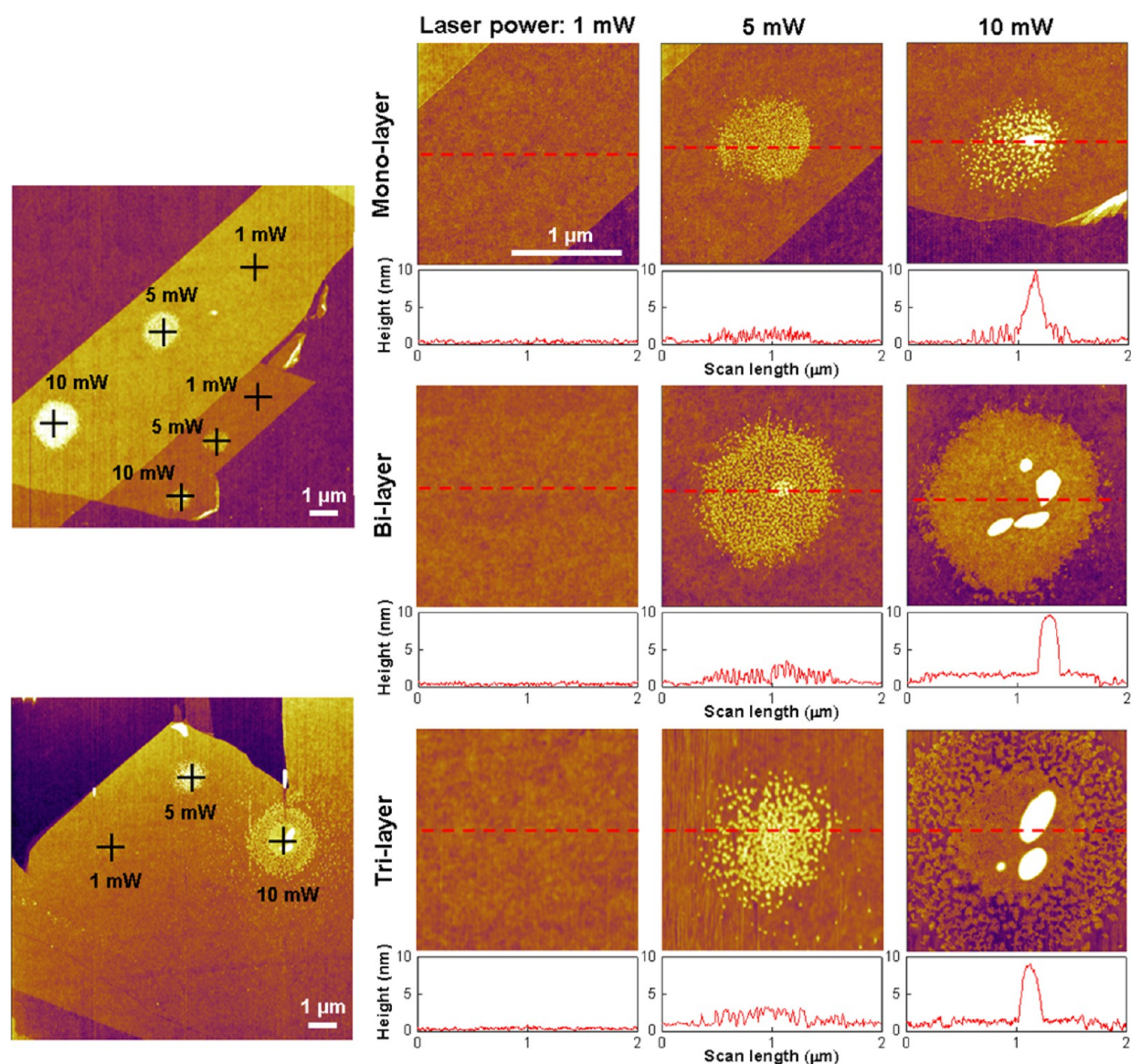


Figure 2. AFM topographic images of 1L, 2L, and 3L MoS₂ obtained by the intermittent contact mode after laser treatments with 1 mW, 5 mW, and 10 mW for 60 s. The locations of laser treatment are indicated by crosses in the low magnification topographic images shown on the left. High magnification topographic images of the laser treated regions are shown on the right along with cross-sectional profiles, which demonstrate increases in particle formation with increasing laser power and number of layers. The red dashed lines in the high magnification topographic images indicate locations where cross-sectional profiles are taken.

the topographies of the MoS₂ specimens were obtained from the intermittent contact mode of AFM. Figure 2 shows topographic images of atomically thin MoS₂ specimens after laser treatment, along with cross-sectional profiles at the centers of the treated regions. As shown in Figure 2, no significant changes in topographic images of the treated regions were observed after treatment with the 1 mW laser, while significant amounts of particles or adsorbates were formed on the MoS₂ surface after treatments with the 5 and 10 mW lasers. The particles or adsorbates were circular in shape, with diameters that generally increased as the number of MoS₂ layers and laser power increased. The diameter of the circular shape formed on 3L MoS₂ by treatment with the 10 mW laser was comparable to the diameter of the laser spot ($\sim 2 \mu\text{m}$). Relatively small particles a few nm in height formed separately on the 1L, 2L, and 3L MoS₂ after treatment with the 5 mW laser and on the 1L MoS₂ after treatment with the 10 mW laser. However, the

circular region in the 2L MoS₂ was almost covered by the particles and a layer about 2 nm in thickness was formed after treatment with the 10 mW laser. As for the 3L MoS₂, a region covered by particles was observed at the center of the laser treated region, surrounded by separately formed particles, after treatment with the 10 mW laser. Furthermore, a few larger particles about 10 nm in height were found at the centers of the treated regions on the 1L, 2L, and 3L MoS₂ after treatment with the 10 mW laser, as clearly demonstrated in the cross-sectional profiles in Figure 2. The volumes of particles approximately calculated from the topographic images increased as the number of layers and laser power increased (Figure S2). The results from 12 different sets of experiments using separately prepared atomically thin MoS₂ specimens showed that the particle formation was reproducible (Figure S3). These outcomes clearly indicate that the particles were generated during laser treatment, and that the degree of particle

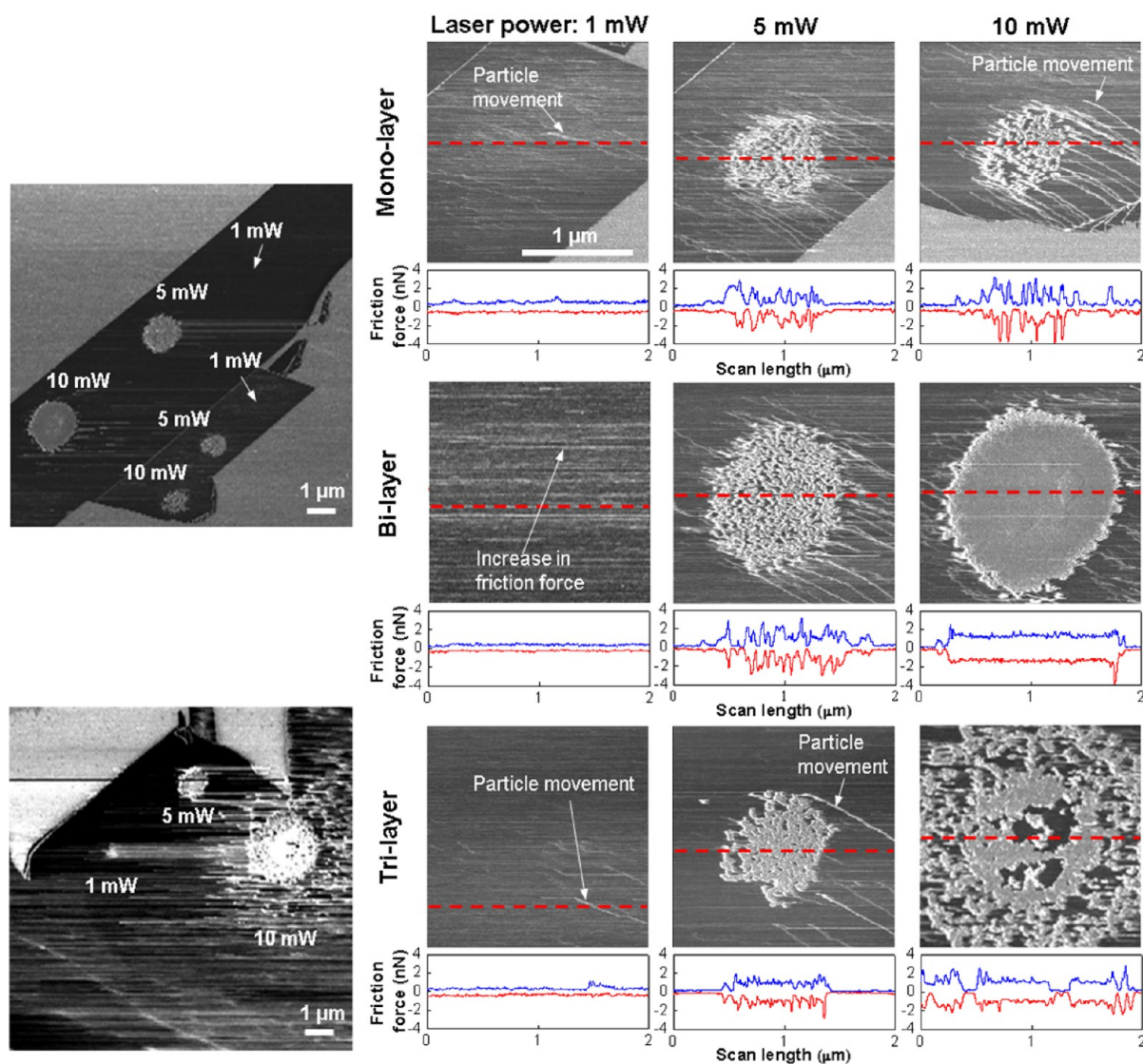


Figure 3. FFM images of 1L, 2L, and 3L MoS₂ obtained by the contact mode under 0.5 nN normal force after laser treatments with 1 mW, 5 mW, and 10 mW for 60 s. The locations of laser treated regions can be clearly identified because of the large friction characteristics of particles based on the low magnification FFM images shown on the left. High magnification FFM images of the laser treated regions are shown on the right along with representative friction loops, which demonstrate increases in friction due to particle formation and signs of particle movement by the AFM probe. In the friction loops, the data obtained from forward and backward scans are shown as blue and red lines, respectively. The red dashed lines in the high magnification topographic images indicate locations where friction loops are taken.

formation increased as the number of layers and laser power increased.

After observation of the topographies of atomically thin MoS₂ specimens after laser treatment, FFM images were obtained with the contact mode of AFM, with an aim to characterize the friction properties of particles and their behavior because of contact sliding. Initially, FFM images were obtained under relatively small normal force. Figure 3 shows FFM images and representative friction loops obtained on the 1L, 2L, and 3L MoS₂ under 0.5 nN normal force. On the basis of the FFM images in Figure 3, regions treated by the laser with 5 and 10 mW, where significant amounts of particles were formed, were clearly identified due to the large friction characteristics of the particles. Particularly, multiple peaks were observed in the friction loops due to separately formed particles on 1L, 2L, and 3L MoS₂ by treatment with the 5 mW laser and on 1L MoS₂ by treatment with the 10 mW laser. In contrast, regions covered with particles on 2L and 3L MoS₂ after

treatment with the 10 mW laser exhibited relatively constant friction forces of about 1 nN. In addition, signs of particle movement by the AFM probe during contact mode imaging were clearly observed in Figure 3. Interestingly, signs of particle movement and an increase in friction force were observed in the high magnification FFM images of regions treated by even the 1 mW laser on 1L and 2L MoS₂ although these regions are not clear in the low magnification FFM image. The region treated by the 1 mW laser on 3L MoS₂ was not clear in the high magnification FFM image although it is clear in low magnification FFM image, but signs of the particle movement are apparent. Considering the particles were moved by the AFM probe and high magnification FFM images were obtained after the low magnification images, the particle movement observed during low magnification FFM imaging may explain why the region treated by the 1 mW laser on 3L MoS₂ was not clearly observed in the high magnification FFM image. Nonetheless, these results indicate that the surfaces of

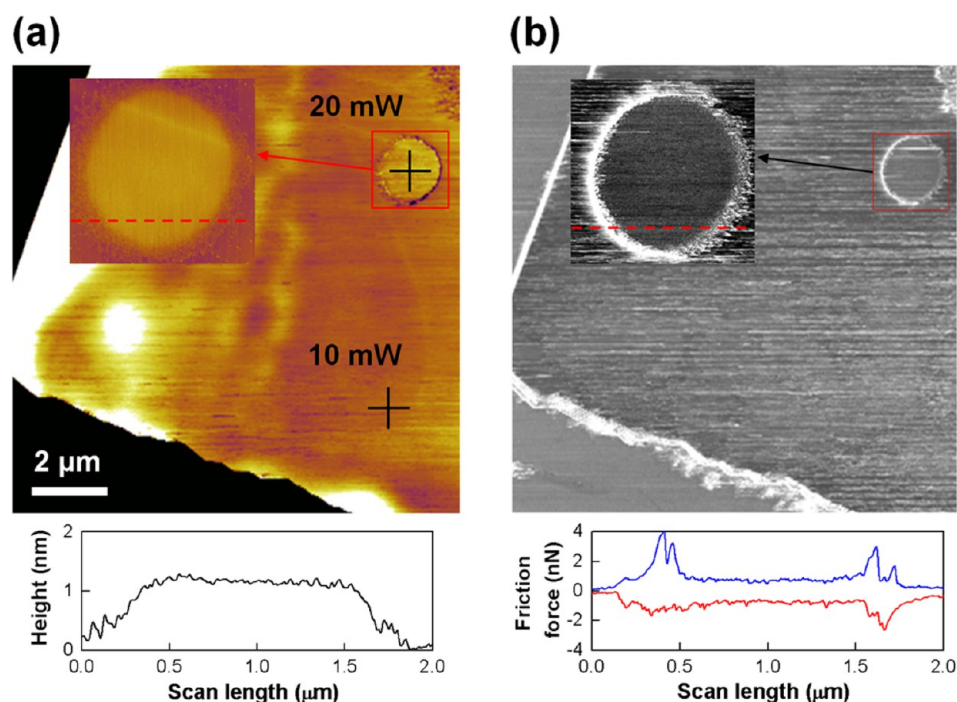


Figure 4. (a) Topographic and (b) FFM images of bulk MoS₂ obtained by intermittent contact and contact modes (under 0.5 nN normal force), respectively, after laser treatments with 10 and 20 mW for 60 s. The locations of the laser treated regions are indicated by crosses in panel a. High magnification topographic and FFM images of the region treated by the 20 mW laser are, respectively, inserted for clarity in panels a and b, along with the cross-sectional profile and the friction loop. The height contrast in the topographic image in panel a is adjusted to clearly observe the top surface of bulk MoS₂.

atomically thin MoS₂ may be affected even by treatment with a 1 mW laser for 60 s, although it is difficult to observe significant changes in topography (Figure 2).

In contrast to the 1L, 2L, and 3L MoS₂, no significant particle formation or increases in friction on the top surface of bulk MoS₂ were observed after laser treatment with powers ranging from 1 to 10 mW. Therefore, the laser power was increased up to 20 mW for the case of bulk MoS₂. Figure 4 shows topographic and FFM images of bulk MoS₂ after laser treatments with powers of 10 mW and 20 mW for 60 s. The topographic image in Figure 4a suggests that the surface of the bulk MoS₂ remained relatively clean without particle formation after treatment at 10 mW. In addition, the FFM image shown in Figure 4b indicates that changes in friction and the appearance and movement of particles were negligible in the regions treated by 10 mW laser, as compared to the untreated regions. However, a layer surrounded by small particles was clearly observed on the region treated by the laser at 20 mW from the topographic images and cross-sectional profile shown in Figure 4a. Furthermore, the FFM image and friction loop in Figure 4 (b) demonstrate that the region treated by the laser at 20 mW exhibited larger friction forces, as expected.

To examine the surfaces of atomically thin MoS₂ beneath the particle formation, the particles formed during laser treatments were moved further by contact mode imaging, following up on the observations of particle mobility as shown in Figure 3. More particles were moved as the applied normal force increased, as expected (Figure S4). Figure 5 shows topographic and FFM images of regions treated by lasers with 5 and 10 mW on 2L MoS₂ obtained after multiple contact mode imaging under normal forces ranging from 0.5 to 7 nN. On the basis of the low magnification topographic images in Figure 5, particles moved by the AFM probe accumulated along the edges of the scanned

regions. However, it was difficult to move relatively large particles formed around the centers of the laser treated regions by contact mode imaging with 7 nN normal force. On the basis of the high magnification topographic images shown in Figure 5, in which the boundaries of the regions with the particles are indicated as dashed lines, the top surfaces of the MoS₂ were clean without significant damage (e.g., height decrease). In addition, the FFM images in Figure 5 showed that differences in the friction forces inside and outside of regions where particles formed, were negligible. These observations indicate that the particles formed by the laser were placed on the top surfaces of MoS₂. To further validate this observation, the presence of the Raman peak at 820 cm⁻¹, which yields MoO₃ on the surface, was carefully examined, considering that bulk MoS₂ is readily oxidized due to the presence of oxygen at high temperature and MoO₃ can thus be formed.⁴⁰ However, the peak intensity at 820 cm⁻¹ in the Raman spectra obtained during laser treatment was not high enough compared to the background intensity to clearly indicate the presence of MoO₃ (Figures S6 and S7), which agrees with the result of previous studies.^{24,26} Hence, it was confirmed that atomically thin MoS₂ was not oxidized by the laser treatments up to 10 mW for 60 s. It is also important to note that the particles were not generated by the substrate, as the atomically thin MoS₂ layer covers the substrate even after laser treatments (Figure 5). Considering that gas molecules may be chemically or physically adsorbed on the MoS₂ surface,^{41–43} particles are likely to originate from the atmosphere as a result of laser treatment of atomically thin MoS₂ in ambient conditions. The initially adsorbed contaminants (e.g., carbon) on the MoS₂ surface (Figure S1) could affect the particle formation, and such contaminants are likely to originate from the environment.^{38,39} AFM topographic images of MoS₂ thinned by thermal annealing in vacuum do

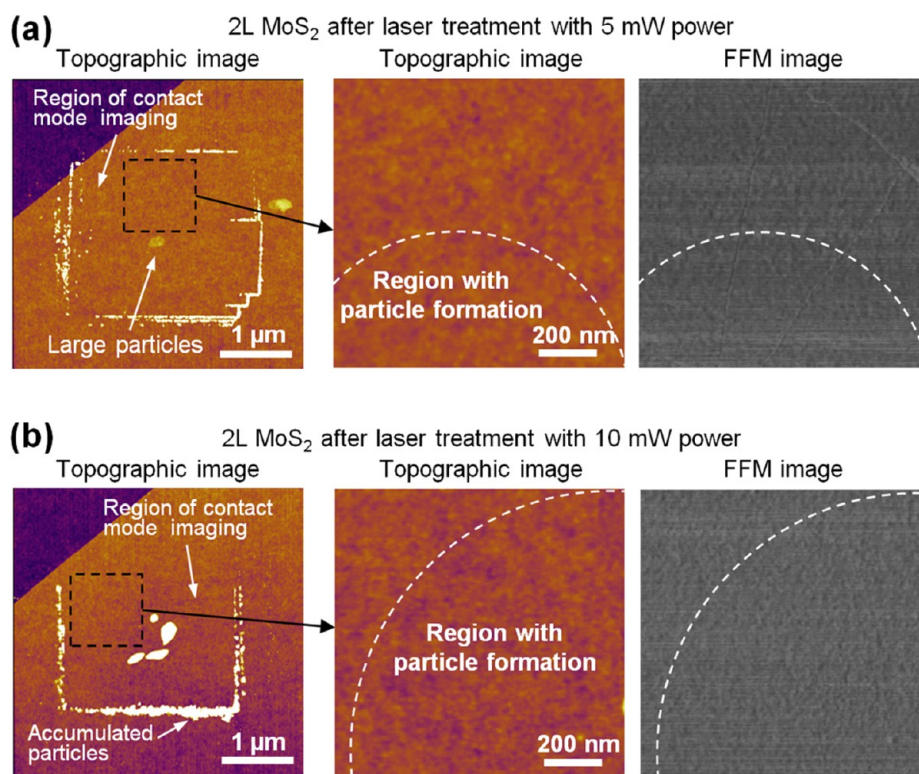


Figure 5. Topographic and FFM images of (a) 2L and (b) 3L MoS₂ after laser treatments with 10 mW followed by contact mode imaging for particle movement. The low magnification topographic images shown on the left indicate that the particles accumulated along the boundaries of regions used for multiple contact mode imaging under 0.5–7 nN normal forces. The dashed boxes in the low magnification topographic images indicate locations of high magnification topographic and FFM images. The boundaries of the region where particles are formed are denoted by dashed lines in the high magnification topographic and FFM images shown on the right.

not show significant particle formation,⁴⁴ which also supports the idea that the particles may originate from the atmosphere.

The dependence of the degree of the particle formation on laser power and the number of layers suggests that particle formation is associated with temperature increases that are influenced by the thermal conductivity of atomically thin MoS₂, interfacial thermal conductance, and heat sink and interference effects of the substrate. In contrast to graphene,⁴⁵ the thermal conductivity of the suspended MoS₂ may be less dependent on thickness since the phonon–phonon scattering channel does not significantly change with respect to thickness.⁴⁶ However, the interfacial thermal conductance between the MoS₂ and substrate may cause the increase in the thermal conductivity of the supported MoS₂.^{19,21} Furthermore, heat may dissipate from atomically thin layers to the substrate, which may act as a heat reservoir.²⁹ It is plausible that the effect of the interfacial thermal conductance and heat dissipation to the substrate decreases as the number of MoS₂ layers increases, which in turn causes increases in temperature at the top surface when the number of layers increases. This may be responsible for the dependence of particle formation on the thickness of the atomically thin MoS₂. By considering that the thermal conductivity of the MoS₂ and interfacial thermal conductance between MoS₂ and SiO₂ may further decrease as the temperature increases,²¹ particle formation may be accelerated by increasing temperature as well. However, as for the bulk MoS₂, the local heat produced by the laser may dissipate more effectively due to the greater thermal conductivity⁴⁷ than that of atomically thin MoS₂.^{18,19,21,46} Furthermore, the bulk MoS₂ may sink heat in more efficient ways than atomically thin MoS₂,

owing to the presence of more than 100 layers. These ideas may explain the relatively high laser powers needed for particle formation on top surface of bulk MoS₂ as shown in Figure 4. This result is also consistent with a previous result, which showed that thick flakes of MoS₂ cannot be easily thinned by laser treatment.²⁴

For comparison, 1L and 2L graphene specimens were treated by a laser up to 40 mW for 60 s and then examined by AFM. However, no significant particle formation or changes in friction force were observed from the topographic and FFM images in the case of graphene (Figures S8 and S9). Because of the significantly greater thermal conductivity of graphene^{45,48–50} compared to atomically thin MoS₂,^{18,19,21,46} graphene is likely to be less susceptible to thermal effects caused by the laser. Note that the laser power density for graphene treatment was approximately 0.16 mW/μm², which is 2 orders of magnitude less than that used to thin graphene.²⁹

With an aim to find the appropriate conditions necessary for Raman spectroscopy to eliminate particle formation, the laser treatment with 0.5 mW was performed. Figure 6 shows AFM topographical and FFM images of 1L MoS₂ before and after treatments with 0.5 mW for 10, 30, and 60 s. To eliminate the possible movement of particles during contact mode imaging, FFM images were carefully obtained at high magnification with no low magnification imaging. The changes in both topography and FFM images after laser treatment for 10 s were negligible. Hence, it was confirmed that the surface of 1L MoS₂ was not affected during the thickness characterization using Raman spectroscopy. However, although no significant alternations of topographical images were observed after laser treatment with

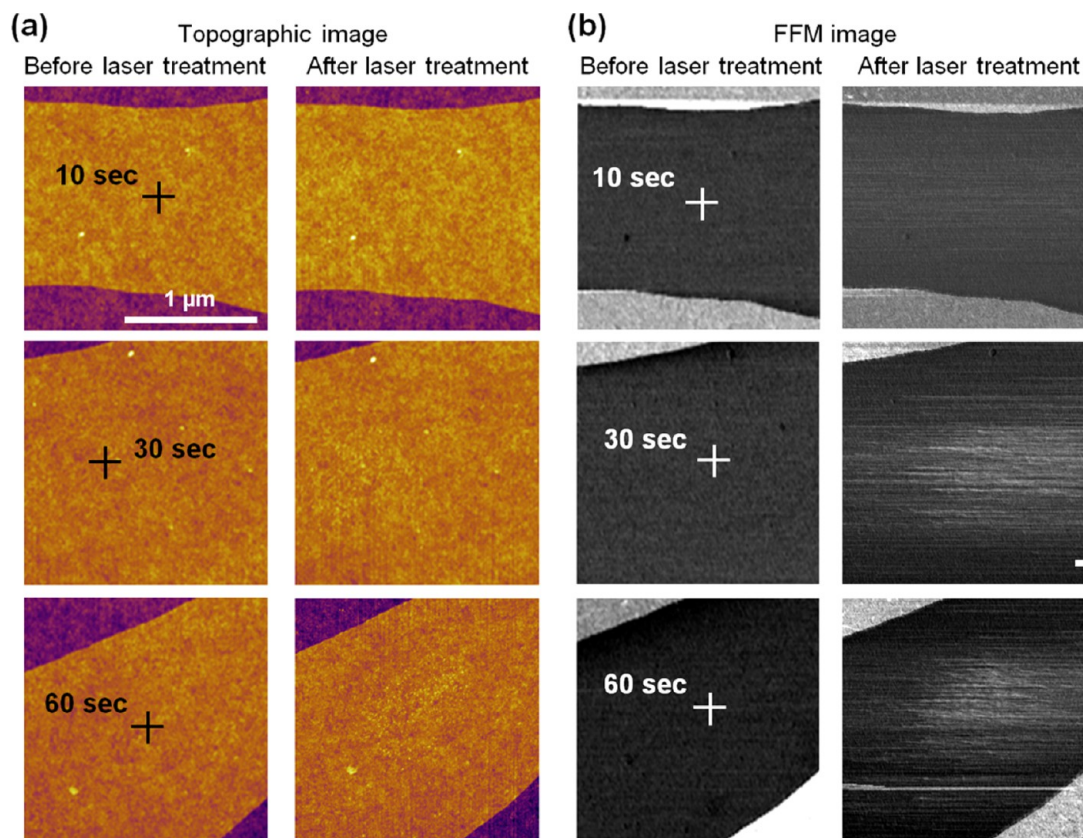


Figure 6. (a) Topographic and (b) FFM images of 1L MoS₂ before and after laser treatments with 0.5 mW for 10, 30, and 60 s. Topographic and FFM images were obtained from the intermittent contact and contact modes of the AFM, respectively. The locations of laser treatment are indicated by crosses in panels a and b.

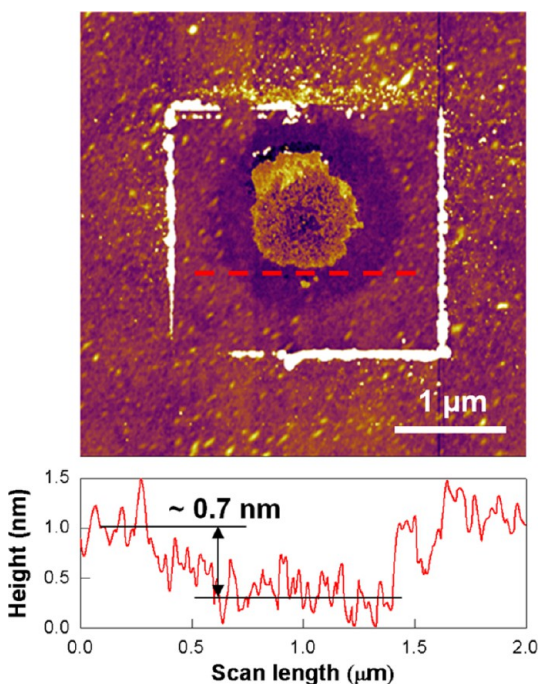


Figure 7. Topographic image and cross-sectional profile of 2L MoS₂ after laser treatment with 20 mW for 60 s followed by contact mode imaging. The cross-sectional profile is provided along with the red dashed line, which shows that the average height decrease is about 0.7 nm.

0.5 mW for 30 and 60 s, the FFM images showed a noticeable increase in friction force in the laser-treated region. The particles adsorbed on 1L MoS₂ were probably too small to be observed in the AFM topographic image after laser treatments with 0.5 mW for 30 and 60 s. The increase in temperature was estimated from Raman spectra obtained during laser treatments (the frequency shift of the A_{1g} mode) and the temperature coefficient for 1L MoS₂ supported on SiO₂ from a previous study.²⁰ The temperatures for the treatments with 0.5, 1, and 5 mW for 60 s were calculated to be about 340, 370, and 450 K, respectively. However, since the Raman spectra obtained for 60 s were used for the temperature calculation, the frequency shift is likely to be underestimated, considering that the temperature increases as the exposure time increases. Therefore, actual temperature for particle formation will be much larger than these values. Nevertheless, based on the results shown in Figure 6, the use of a laser with less than 0.5 mW for less than 10 s is recommended to eliminate thermal effects on 1L MoS₂ during Raman spectral measurements.

To observe the thinning of atomically thin MoS₂ by laser treatment, 2L MoS₂ was treated by a laser with 20 mW for 60 s and examined by AFM. Figure 7 shows topographic image of 2L MoS₂ after laser treatment followed by multiple contact mode imaging for particle movement from the treated region, along with a cross-sectional profile. More particles remained than in the data shown in Figure 5, although the normal force applied by the AFM probe increased up to 15 nN during contact mode imaging. However, the topographic image shown in Figure 7 demonstrates the thinning of 2L MoS₂ around the region where the particles remained. The cross-sectional profile

shown in Figure 7 indicates that the decrease in height of the thinned region is about 0.7 nm, which corresponds to the thickness of 1L MoS₂. The thinning of the MoS₂ layer occurred, probably due to sublimation,^{24,26} after particle formation as the temperature increased with increasing laser power. The laser power required for thinning 2L MoS₂ in this work is relatively larger than that used for thinning of about 20L MoS₂ in a previous study.²⁴ However, an increase in the degree of the particle formation with number of layers at a given laser treatment condition (Figure 2) suggests that temperature may increase more as the number of layers increases to a certain level, due to decreases in the effect of the interfacial thermal conductance and heat dissipation to the substrate, which may in turn decrease the laser power required for the thinning relatively thick MoS₂.

The spot size and intensity of the laser, as well as the degree of the focusing of laser on the top surface of atomically thin MoS₂, may affect the local temperature, which in turn influences the degree of particle formation. Furthermore, the thermal conductivity of atomically thin MoS₂ may be affected by the quality of the specimen associated with the preparation method (e.g., mechanical exfoliations vs chemical vapor deposition).^{18,19,21} Therefore, the measurement conditions required for Raman spectroscopy to eliminate the particle formation may vary. However, the experimental results suggest that, for typical Raman spectral measurements in ambient conditions, the use of laser power below 0.5 mW with exposure time less than 10 s is recommended to eliminate thermal effects on 1L MoS₂. Considering that lasers with powers ranging from 0.14 mW to 2 mW have been used to characterize atomically thin MoS₂ in other work,^{16,18,19,21,24} this information provides a guideline to minimize thermal effects during Raman spectral measurements. This work also provides useful input for the design of nanodevices based on atomically thin MoS₂. For example, considering the fact that particle adsorption or contamination may degrade the performance of nanodevices based on atomically thin MoS₂,^{2,42} temperature increase during fabrication and operation should be minimized to prolong life and improve device performance. Furthermore, to promote the use of atomically thin MoS₂ as a lubricant layer for nanodevices with contact sliding, the increase in temperature due to contact sliding should be taken into account since it may cause increases in friction due to particle formation, especially in ambient conditions.

CONCLUSION

This work presents an investigation of thermal effects caused by lasers on the surface of atomically thin MoS₂. Atomically thin MoS₂ with the various thicknesses were treated with lasers ranging in power from 0.5 to 20 mW using Raman spectroscopy, and the treated regions were then carefully observed by FFM as well as topographic images via AFM. It was found that the particles, which are likely to originate from the atmosphere, may be adsorbed on the top surface of atomically thin MoS₂ due to laser-induced thermal effects. Also, it was observed that the degree of particle formation increased as the number of MoS₂ layers and laser power increased. In addition, the thinning of atomically thin MoS₂ occurred after particle formation, as laser power further increased up to 20 mW. The thickness dependence observed in terms of particle formation suggests that the thermal behavior of the supported atomically thin MoS₂ may differ with respect to the number of layers. Based on the experimental results, laser power and

exposure time are recommended to eliminate thermal effects on 1L MoS₂ during Raman spectral measurements. The results from this work provide important information for the thermal design of atomically thin MoS₂-based devices with prolonged life and improved performance.

ASSOCIATED CONTENT

Supporting Information

The Supporting Information is available free of charge on the ACS Publications website at DOI: 10.1021/acsami.5b09382.

Particle formation with respect to the number of MoS₂ layer and laser power, AFM and FFM images showing reproducible particle formation by laser treatment, AFM and FFM images showing movement of particles caused by the AFM probe, Raman spectra of atomically thin MoS₂ along with a spatial map of integrated spectra after laser treatment, and AFM and FFM images showing no significant particle formation on monolayer graphene after laser treatment (PDF)

AUTHOR INFORMATION

Corresponding Author

*Tel: +82-52-259-2744. Fax: +82-52-259-1680. Email: khchung@ulsan.ac.kr.

Present Address

[†](S.T.C.) School of Mechanical Engineering, Chung-Ang University, Seoul 06974, Republic of Korea.

Notes

The authors declare no competing financial interest.

ACKNOWLEDGMENTS

This research was supported by the Basic Science Research Program through the National Research Foundation of Korea (NRF), funded by the Ministry of Education (NRF-2014R1A1A2058201). Specific commercial equipment, instruments, and materials that are identified in this report are listed in order to adequately describe the experimental procedure and are not intended to imply endorsement or recommendation by the National Institute of Standards and Technology.

REFERENCES

- (1) Kuc, A.; Zibouche, N.; Heine, T. Influence of Quantum Confinement on the Electronic Structure of the Transition Metal Sulfide TS₂. *Phys. Rev. B: Condens. Matter Mater. Phys.* **2011**, *83*, 245213.
- (2) Radisavljevic, B.; Radenovic, A.; Brivio, J.; Giacometti, V.; Kis, A. Single-layer MoS₂ Transistors. *Nat. Nanotechnol.* **2011**, *6*, 147–150.
- (3) Radisavljevic, B.; Whitwick, M. B.; Kis, A. Integrated Circuits and Logic Operations Based on Single-Layer MoS₂. *ACS Nano* **2011**, *5*, 9934–9938.
- (4) Yin, Z.; Li, H.; Li, H.; Jiang, L.; Shi, Y.; Sun, Y.; Lu, G.; Zhang, Q.; Chen, X.; Zhang, H. Single-Layer MoS₂ Phototransistors. *ACS Nano* **2012**, *6*, 74–80.
- (5) Lee, H. S.; Min, S.; Chang, Y.; Park, M. K.; Nam, T.; Kim, H.; Kim, J. H.; Ryu, S.; Im, S. MoS₂ Nanosheet Phototransistors with Thickness-Modulated Optical Energy Gap. *Nano Lett.* **2012**, *12*, 3695–3700.
- (6) Li, H.; Yin, Z.; He, Q.; Li, H.; Huang, X.; Lu, G.; Fam, D. W. H.; Tok, A. I. Y.; Zhang, Q.; Zhang, H. Fabrication of Single- and Multilayer MoS₂ Film-Based Field-Effect Transistors for Sensing NO at Room Temperature. *Small* **2012**, *8*, 63–67.
- (7) Perkins, F. K.; Friedman, A. L.; Cobas, E.; Campbell, P. M.; Jernigan, G. G.; Jonker, B. T. Chemical Vapor Sensing with Monolayer MoS₂. *Nano Lett.* **2013**, *13*, 668–673.

- (8) Bertolazzi, S.; Brivio, J.; Kis, A. Stretching and Breaking of Ultrathin MoS₂. *ACS Nano* **2011**, *5*, 9703–9709.
- (9) Castellanos-Gomez, A.; Poot, M.; Steele, G. A.; van der Zant, H. S. J.; Agrait, N.; Rubio-Bollinger, G. Elastic Properties of Freely Suspended MoS₂ Nanosheets. *Adv. Mater.* **2012**, *24*, 772–775.
- (10) Martin, J. M.; Donnet, C.; Le Mogne, T.; Epicier, T. Superlubricity of Molybdenum Disulfide. *Phys. Rev. B: Condens. Matter Phys.* **1993**, *48*, 10583–10586.
- (11) Lee, C.; Li, Q.; Kalb, W.; Liu, X.; Berger, H.; Carpick, R. W.; Hone, J. Frictional Characteristics of Atomically Thin Sheets. *Science* **2010**, *328*, 76–80.
- (12) Quereda, J.; Castellanos-Gomez, A.; Agrait, N.; Rubio-Bollinger, G. Single-layer MoS₂ Roughness and Sliding Friction Quenching by Interaction with Atomically Flat Substrates. *Appl. Phys. Lett.* **2014**, *105*, 053111.
- (13) Donnet, C.; Erdemir, A. Solid Lubricant Coatings: Recent Developments and Future Trends. *Tribol. Lett.* **2004**, *17*, 389–397.
- (14) Sen, H. S.; Sahin, H.; Peeters, F. M.; Durgun, E. Monolayers of MoS₂ as an Oxidation Protective Nanocoating Material. *J. Appl. Phys.* **2014**, *116*, 083508.
- (15) Lee, C.; Yan, H.; Brus, L. E.; Heinz, T. F.; Hone, J.; Ryu, S. Anomalous Lattice Vibrations of Single- and Few-Layer MoS₂. *ACS Nano* **2010**, *4*, 2695–2700.
- (16) Li, H.; Zhang, Q.; Yap, C. C. R.; Tay, B. K.; Edwin, T. H. T.; Olivier, A.; Baillargeat, D. From Bulk to Monolayer MoS₂: Evolution of Raman Scattering. *Adv. Funct. Mater.* **2012**, *22*, 1385–1390.
- (17) Lanzillo, N. A.; Glen Birdwell, A.; Amani, M.; Crowne, F. J.; Shah, P. B.; Najmaei, S.; Liu, Z.; Ajayan, P. M.; Lou, J.; Dubey, M.; Nayak, S. K.; O'Regan, T. P. Temperature-Dependent Phonon Shifts in Monolayer MoS₂. *Appl. Phys. Lett.* **2013**, *103*, 093102.
- (18) Sahoo, S.; Gaur, A. P. S.; Ahmadi, M.; Guinel, M. J.-F.; Katiyar, R. S. Temperature-Dependent Raman Studies and Thermal Conductivity of Few-Layer MoS₂. *J. Phys. Chem. C* **2013**, *117*, 9042–9047.
- (19) Yan, R.; Simpson, J. R.; Bertolazzi, S.; Brivio, J.; Watson, M.; Wu, X.; Kis, A.; Luo, T.; Hight Walker, A. R.; Xing, H. G. Thermal Conductivity of Monolayer Molybdenum Disulfide Obtained from Temperature-Dependent Raman Spectroscopy. *ACS Nano* **2014**, *8*, 986–993.
- (20) Taube, A.; Judek, J.; Jastrzębski, C.; Duzynska, A.; Świtkowski, K.; Zdrojek, M. Temperature-Dependent Nonlinear Phonon Shifts in a Supported MoS₂ Monolayer. *ACS Appl. Mater. Interfaces* **2014**, *6*, 8959–8963.
- (21) Taube, A.; Judek, J.; Łapińska, A.; Zdrojek, M. Temperature-Dependent Thermal Properties of Supported MoS₂ Monolayers. *ACS Appl. Mater. Interfaces* **2015**, *7*, 5061–5065.
- (22) Zhang, X.; Sun, D.; Li, Y.; Lee, G.; Cui, X.; Chenet, D.; You, Y.; Heinz, T. F.; Hone, J. C. Measurement of Lateral and Interfacial Thermal Conductivity of Single- and Bilayer MoS₂ and MoSe₂ Using Refined Optothermal Raman Technique. *ACS Appl. Mater. Interfaces* **2015**, *7*, 25923–25929.
- (23) Najmaei, S.; Liu, Z.; Ajayan, P. M.; Lou, J. Thermal Effects on the Characteristic Raman Spectrum of Molybdenum Disulfide (MoS₂) of Varying Thicknesses. *Appl. Phys. Lett.* **2012**, *100*, 013106.
- (24) Castellanos-Gomez, A.; Barkelid, M.; Goossens, A. M.; Calado, V. E.; van der Zant, H. S. J.; Steele, G. A. Laser-Thinning of MoS₂: On Demand Generation of a Single-Layer Semiconductor. *Nano Lett.* **2012**, *12*, 3187–3192.
- (25) Lu, J.; Lu, J. H.; Liu, H.; Liu, B.; Chan, K. X.; Lin, J.; Chen, W.; Loh, K. P.; Sow, C. H. Improved Photoelectrical Properties of MoS₂ Films after Laser Micromachining. *ACS Nano* **2014**, *8*, 6334–6343.
- (26) Paradisanos, I.; Kymakis, E.; Fotakis, C.; Kioseoglou, G.; Stratakis, E. Intense Femtosecond Photoexcitation of Bulk and Monolayer MoS₂. *Appl. Phys. Lett.* **2014**, *105*, 041108.
- (27) Gupta, R.; Xiong, Q.; Adu, C. K.; Kim, U. J.; Eklund, P. C. Laser-Induced Fano Resonance Scattering in Silicon Nanowires. *Nano Lett.* **2003**, *3*, 627–631.
- (28) Sahoo, S.; Arora, A. K. Laser-Power-Induced Multiphonon Resonant Raman Scattering in Laser-Heated CdS Nanocrystal. *J. Phys. Chem. B* **2010**, *114*, 4199–4203.
- (29) Han, G. H.; Chae, S. J.; Kim, E. S.; Güneş, F.; Lee, I. H.; Lee, S. W.; Lee, S. Y.; Lim, S. C.; Jeong, H. K.; Jeong, M. S.; Lee, Y. H. Laser Thinning for Monolayer Graphene Formation: Heat Sink and Interference Effect. *ACS Nano* **2011**, *5*, 263–268.
- (30) Lin, L.; Kim, D.; Kim, W.; Jun, S. Friction and Wear Characteristics of Multi-Layer Graphene Films Investigated by Atomic Force Microscopy. *Surf. Coat. Technol.* **2011**, *205*, 4864–4869.
- (31) Kwon, S.; Ko, J.; Jeon, K.; Kim, Y.; Park, J. Y. Enhanced Nanoscale Friction on Fluorinated Graphene. *Nano Lett.* **2012**, *12*, 6043–6048.
- (32) Choi, J. S.; Kim, J.; Byun, I.; Lee, D. H.; Lee, M. J.; Park, B. H.; Lee, C.; Yoon, D.; Cheong, H.; Lee, K. H.; Son, Y.; Park, J. Y.; Salmeron, M. Friction Anisotropy-Driven Domain Imaging on Exfoliated Monolayer Graphene. *Science* **2011**, *333*, 607–610.
- (33) Cho, D.; Wang, L.; Kim, J.; Lee, G.; Kim, E. S.; Lee, S.; Lee, S. Y.; Hone, J.; Lee, C. Effect of Surface Morphology on Friction of Graphene on Various Substrates. *Nanoscale* **2013**, *5*, 3063–3069.
- (34) Novoselov, K. S.; Geim, A. K.; Morozov, S. V.; Jiang, D.; Zhang, Y.; Dubonos, S. V.; Grigorieva, I. V.; Firsov, A. A. Electric Field Effect in Atomically Thin Carbon Films. *Science* **2004**, *306*, 666–669.
- (35) Hutter, J. L.; Bechhoefer, J. Calibration of Atomic-Force Microscope Tips. *Rev. Sci. Instrum.* **1993**, *64*, 1868–1873.
- (36) Tran Khac, B. C.; Chung, K. – H. Quantitative Assessment of Contact and Non-Contact Lateral Force Calibration Methods for Atomic Force Microscopy. *Ultramicroscopy* **2016**, *161*, 41–50.
- (37) Nemes-Incze, P.; Osváth, Z.; Kamarás, K.; Biró, L. P. Anomalies in Thickness Measurements of Graphene and Few Layer Graphite Crystals by Tapping Mode Atomic Force Microscopy. *Carbon* **2008**, *46*, 1435–1442.
- (38) Azcatl, A.; McDonnell, S.; Santosh, K. C.; Peng, X.; Dong, H.; Qin, X.; Addou, R.; Mordi, G. I.; Lu, N.; Kim, J.; Kim, M. J.; Cho, K.; Wallace, R. M. MoS₂ Functionalization for Ultra-Thin Atomic Layer Deposited Dielectrics. *Appl. Phys. Lett.* **2014**, *104*, 111601.
- (39) Addou, R.; McDonnell, S.; Barrera, D.; Guo, Z.; Azcatl, A.; Wang, J.; Zhu, H.; Hinkle, C. L.; Quevedo-Lopez, M.; Alshareef, H. N.; Colombo, L.; Hsu, J. W. P.; Wallace, R. M. Impurities and Electronic Property Variations of Natural MoS₂ Crystal Surfaces. *ACS Nano* **2015**, *9*, 9124–9133.
- (40) Windom, B.; Sawyer, W. G.; Hahn, D. A Raman Spectroscopic Study of MoS₂ and MoO₃: Applications to Tribological Systems. *Tribol. Lett.* **2011**, *42*, 301–310.
- (41) Davis, S. M.; Carver, J. C. Oxygen Chemisorption at Defect Sites in MoS₂ and ReS₂ Basal Plane Surfaces. *Appl. Surf. Sci.* **1984**, *20*, 193–198.
- (42) Qiu, H.; Pan, L.; Yao, Z.; Li, J.; Shi, Y.; Wang, X. Electrical Characterization of Back-Gated Bi-Layer MoS₂ Field-Effect Transistors and the Effect of Ambient on Their Performances. *Appl. Phys. Lett.* **2012**, *100*, 123104.
- (43) Yue, Q.; Shao, Z.; Chang, S.; Li, J. Adsorption of Gas Molecules on Monolayer MoS₂ and Effect of Applied Electric Field. *Nanoscale Res. Lett.* **2013**, *8*, 425.
- (44) Lu, X.; Utama, M. I. B.; Zhang, J.; Zhao, Y.; Xiong, Q. Layer-by-Layer Thinning of MoS₂ by Thermal Annealing. *Nanoscale* **2013**, *5*, 8904–8908.
- (45) Ghosh, S.; Bao, W.; Nika, D. L.; Subrina, S.; Pokatilov, E. P.; Lau, C. N.; Balandin, A. A. Dimensional Crossover of Thermal Transport in Few-Layer Graphene. *Nat. Mater.* **2010**, *9*, 555–558.
- (46) Ding, Z.; Jiang, J. – W.; Pei, Q. – X.; Zhang, Y. – W. In-Plane and Cross-Plane Thermal Conductivities of Molybdenum Disulfide. *Nanotechnology* **2015**, *26*, 065703.
- (47) Liu, J.; Choi, G.; Cahill, D. G. Measurement of the Anisotropic Thermal Conductivity of Molybdenum Disulfide by the Time-Resolved Magneto-Optic Kerr Effect. *J. Appl. Phys.* **2014**, *116*, 233107.
- (48) Balandin, A. A.; Ghosh, S.; Bao, W.; Calizo, L.; Teweldebrhan, D.; Miao, F.; Lau, C. N. Superior Thermal Conductivity of Single-Layer Graphene. *Nano Lett.* **2008**, *8*, 902–907.
- (49) Ghosh, S.; Calizo, L.; Teweldebrhan, D.; Pokatilov, E. P.; Nika, D. L.; Balandin, A. A.; Bao, W.; Miao, F.; Lau, C. N. Extremely High Thermal Conductivity of Graphene: Prospects for Thermal Manage-

ment Applications in Nanoelectronic Circuits. *Appl. Phys. Lett.* **2008**, *92*, 151911.

(50) Seol, J. H.; Jo, I.; Moore, A. L.; Lindsay, L.; Aitken, Z. H.; Pettes, M. T.; Li, X.; Yao, Z.; Huang, R.; Broido, D.; Mingo, N.; Ruoff, R. S.; Shi, L. Two-Dimensional Phonon Transport in Supported Graphene. *Science* **2010**, *328*, 213–216.